Science

RESEARCH ARTICLES

Cite as: K. Singh *et al.*, *Science*
10.1126/science.ade5337 (2023).

Mid-circuit correction of correlated phase errors using an array of spectator qubits

K. Singh[1]†, C. E. Bradley[2]†, S. Anand[2]†, V. Ramesh[3], R. White[3], H. Bernien[2]*

[1]Intelligence Community Postdoctoral Research Fellowship Program, Pritzker School of Molecular Engineering, University of Chicago, Chicago, IL 60637, USA. [2]Pritzker School of Molecular Engineering, University of Chicago, Chicago, IL 60637, USA. [3]Department of Physics, University of Chicago, Chicago, IL 60637, USA.

†These authors contributed equally to this work. *Corresponding author. Email: bernien@uchicago.edu

Scaling up invariably error-prone quantum processors is a formidable challenge. Although quantum error correction ultimately promises fault-tolerant operation, the required qubit overhead and error thresholds are daunting. In a complementary proposal, co-located, auxiliary 'spectator' qubits act as in-situ probes of noise, and enable real-time, coherent corrections of data qubit errors. We use an array of cesium spectator qubits to correct correlated phase errors on an array of rubidium data qubits. By combining in-sequence readout, data processing, and feed-forward operations, these correlated errors are suppressed within the execution of the quantum circuit. The protocol is broadly applicable to quantum information platforms, and establishes key tools for scaling neutral-atom quantum processors: mid-circuit readout of atom arrays, real-time processing and feed-forward, and coherent mid-circuit reloading of atomic qubits.

Realizing large-scale programmable quantum systems that can overcome inevitable noise sources is a central challenge for modern physics (*1*, *2*). Environmental noise and experimental parameter drift necessitate strategies to reduce their impact and overcome resulting qubit errors. Although quantum error correction will ultimately be required, achieving the necessary qubit operation fidelities is an outstanding challenge for present quantum computing platforms (*3*–*9*). Moreover, the effectiveness of error correction codes is reduced by correlated errors (*10*, *11*), which may naturally occur when the qubits are in close spatial proximity or are controlled by shared hardware (*12*–*16*).

To address these challenges, a number of techniques have been developed to mitigate the effects of noise, such as composite pulses (*17*), optimal control (*18*), dynamical decoupling (*17*, *19*), Hamiltonian learning (*20*), and machine-learning-based control engineering (*21*). These techniques have found great success, but they are typically tailored to specific noise models or require careful calibration, and thus face challenges when employed in realistic, fluctuating environments. For example, dynamical decoupling generates a filter function that mitigates a particular spectrum of noise, with passbands remaining that are not suppressed (*22*). Additionally, it is only effective if the correlation time of the noise is long with respect to the interpulse delay.

Recent theoretical work has proposed a complementary technique based on 'spectator' qubits: additional qubits that are co-located with the computational 'data' qubits and are susceptible to the same noise sources. Spectator qubits act as in-situ probes of that noise, such that measurement and feed-forward can be used to coherently protect the data qubits during the execution of a quantum algorithm (*23*–*25*). Notably, under two key conditions, spectator protocols are agnostic to the spectrum and correlation time of the noise source. First, the noise-induced dynamics must be correlated between the spectator and data qubits. Second, an estimate of those dynamics must be made by reading out the spectator qubits — and a subsequent feed-forward operation applied — much faster than the timescale over which the data and spectator qubits decorrelate. This second requirement has limited the experimental implementation of such protocols, as a significant number of measurements are required to reliably estimate the effects of a dynamic noise environment. Furthermore, the spectator qubit readouts must be performed mid-circuit without perturbing the data qubits.

Here, we overcome these challenges and demonstrate real-time correction of correlated phase errors using a dual-species array of individually trapped neutral atoms. The protocol is outlined in Fig. 1A. Data qubits (rubidium atoms) and spectator qubits (cesium atoms) are laser-cooled into optical tweezer arrays (*26*). During logic operations on the data qubits, mid-circuit readouts on the array of ~60 spectator qubits enable single-shot estimation of globally correlated phase errors. The readout results are processed in real-time and used to infer the noise-induced phase accrued by the ~60 data qubits. Crucially, owing to the crosstalk-free operation of the two species, these readouts do not disturb the coherence of the data qubits. We leverage a classical control architecture to perform in-sequence feed-forward, such that correlated errors on the data qubits are mitigated within the execution of the quantum circuit. Finally, we show that the spectator qubits can be replenished within the data qubit coherence time, an essential step toward repeated measurements and the continuous operation of atom-based quantum processors.

Mid-circuit readout of spectator qubits

Our experiment is performed on arrays of 10x10 and 11x11 sites for the spectator and data qubits respectively (Fig. 1B), which are stochastically loaded with an average loading fraction of ~55%. The experimental apparatus has been upgraded from our previous work (*26*) to incorporate qubit initialization, manipulation, and readout, along with classical hardware to implement real-time processing and feed-forward. Here, the qubits are encoded into long-lived hyperfine states ($|F=1, m_F=0\rangle := |0\rangle_{Rb}$ and $|F=2, m_F=0\rangle := |1\rangle_{Rb}$ for Rb; $|F=3, m_F=0\rangle := |0\rangle_{Cs}$ and $|F=4, m_F=0\rangle := |1\rangle_{Cs}$ for Cs). Microwave driving of the data and spectator qubits after optical pumping into $|1\rangle_{Rb}$ and $|1\rangle_{Cs}$ reveals coherent Rabi oscillations (Fig. 1C).

An essential ingredient for the spectator protocol is to perform mid-circuit readout (MCR) of the spectator qubits without inducing additional data qubit decoherence. This is challenging in single-species atom arrays because all atoms are resonant with the excitation laser, and the measured qubits scatter light which can decohere the data qubits via reabsorption. To overcome this, several ideas have been proposed and demonstrated, including coherently transporting qubits into readout cavities (*27*), or using additional shelving states to hide atoms from excitations from the readout light, as demonstrated for trapped ions (*4*). However, realizing crosstalk-free imaging in large atom arrays has remained an outstanding challenge. A key motivation behind the dual-species approach is that the different atomic species have distinct optical transitions, and measurements on one species are not expected to influence the other (*26*, *28*).

In a first experiment, we characterize the spectator qubit mid-circuit readout, and measure its impact on the data qubit coherence. The quantum circuit is shown in Fig. 2A. During an XY8 decoupling sequence on the data qubits, an XY4 sequence is performed on the spectators. The spectator qubits are measured within the XY8 sequence by selectively removing all atoms in the $|1\rangle_{Cs}$ state via a resonant laser pulse and then fluorescence imaging for 15 ms. The coherence of the data and spectator qubits as a function of their individual decoupling times are shown in Fig. 2, B and E, respectively. While the camera exposure time is fixed, the imaging light is applied for a variable time, 5τ (of a total of 16τ) in order to determine its effect on the data qubits. Crucially, the data qubit coherence time is unaltered by the MCR [fitted $T_{2,MCR}^{XY8}$ = 0.68(1) s, $T_{2,No\ MCR}^{XY8}$ = 0.65(2) s]. The large detuning of the imaging light leads to negligibly low spontaneous scattering rates of ~10^{-7} Hz. Moreover, spontaneous Raman scattering events which change these m_F states are further suppressed by a factor of 0.009 due to destructive interference of the off-resonant transition amplitudes (*12*). The theoretical T_1 time from this decay channel is thus ~10^8 s, resulting in a data qubit bit flip rate from readout crosstalk of ~10^{-11} during the 15 ms MCR. This readout duration was chosen to balance the requirements for achieving a high discrimination fidelity while minimizing the time for a feed-forward operation (*29*) The discrimination fidelity of the spectator qubit states (Fig. 2D) is extracted from a bimodal fit to the fluorescence histogram of each spectator qubit, as exemplified in Fig. 2C. Across the spectator array we find a mean fidelity of 0.989(5), showing that the spectator qubit states are well-resolved by MCR.

Spectator protocol and correction of phase errors

The preservation of data qubit coherence during spectator readout opens the possibility for feed-forward operations within a quantum circuit. Under simultaneous evolution, noise channels can induce correlated phase errors between the data and spectator qubits. Importantly, the large number of spectator qubits allows single-shot estimation of the acquired phase from one simultaneous MCR. The phase accrued by the data qubits can then be inferred and corrected in real-time, as illustrated in Fig. 3A.

To demonstrate this capability, we inject global magnetic field noise with amplitudes and frequencies comparable to those typically found in laboratory environments. The phase of the noise is random in each experimental repetition, without shot-to-shot temporal correlations. We focus on monochromatic noise for ease of synthesis and interpretation of protocol performance, but note that our scheme is generally agnostic to the noise spectrum. The pulse sequence for the experiment is shown in Fig. 3B. The data and spectator qubits undergo synchronous dynamical decoupling and acquire correlated errors from the common noise. Although the filter function of the CPMG-type dynamical decoupling sequence partially mitigates such noise, certain frequencies still couple into the sequence, occurring at odd-harmonics of $f_{AC} = 1/(4\tau)$ = 36.2 Hz, where 2τ is the time between π-pulses (*22*). The spectators sample this noise for three-quarters of the total evolution time of the data qubits, with the remainder of the time assigned for MCR and feed-forward. To achieve fast camera processing and feedback, we utilize a camera-linked classical control architecture for in-sequence processing of the fluorescence images, which in turn triggers an arbitrary-waveform-generator to perform real-time updates of the phase of the final data qubit π/2-pulse (*29*). The phase update of this final π/2-pulse is equivalent to a *Z*-axis qubit rotation, which is used to correct the noise-induced phase error on the data qubits.

To estimate the phase acquired by the spectators, Φ_S, MCR is performed along an axis orthogonal to the state preparation axis. Accordingly, the collective expectation value of the array can be inverted to give an estimate, $\Phi'_S = \arcsin\left(\langle\sigma_y\rangle / C\right)$, where C is a scaling factor describing the amplitude of the signal in the absence of injected noise (*29*). Φ'_S is uniquely defined when the accrued phase lies within [−π/2, π/2], beyond which the protocol breaks down. The estimated noise-induced phase accrued by the data qubits is given by $\Phi'_D = \gamma\beta\Phi'_S$, where $\gamma = 4/3$ is the ratio of the sensing times and $\beta = 1.35$ is the ratio of the second-order Zeeman shifts of the clock states (*29*). With this knowledge, a real-time correction can be applied.

We first probe the case for which the noise is maximally coupled, at f_{AC} (10.7 mG RMS). Without the spectator protocol, the random phase of the noise leads to complete dephasing of the data qubits. Strikingly, the feed-forward corrects the noise-induced phase in each experimental repetition, resulting in a recovery of the data qubit coherence (Fig. 3C). The coherence as a function of the noise amplitude is shown in Fig. 3D. In stark contrast to the rapid decay observed in the absence of feed-forward, the spectator protocol robustly preserves coherence for field strengths below 11 mG. Beyond this value, the accrued phases on the spectator qubits can exceed ±π/2, where the protocol can no longer unambiguously detect phase errors.

Next, we study the dependence on the noise frequency for an RMS noise strength of 10.7 mG (Fig. 3E). For a range of frequencies close to f_{AC}, real-time correction results in an absolute gain in the measured signal, shielding the data qubits from otherwise deleterious decoherence. A pair of small additional features occur near f_{AC} in the 'feed-forward on' spectrum, arising from the finite spectator readout time, which leads to decorrelation between the data and spectator qubits. Reducing the fraction of time used for MCR would suppress these effects. Outside this region, feed-forward causes a slight reduction in the measured coherence resulting from imperfect phase estimation. For both the amplitude and frequency sweep, the salient features of the data are well described by simple simulations of the experiment with no free parameters aside from a global amplitude rescaling (Fig. 3, D and E). These are based on the assumption of monochromatic noise that solely perturbs the frequencies of the qubits (*29*). At stronger noise strengths, a slight discrepancy occurs, which likely arises from a breakdown of these assumptions.

Alongside our numerical simulations, analytic expressions can be derived for the error due to quantum projection noise (QPN) in the phase estimation step. In the absence of any correlated dephasing, QPN-induced feed-forward errors modulate the data qubit expectation values $\langle\sigma_x\rangle$ by $f \approx 1 - \frac{\gamma^2\beta^2}{2NC^2}$ (*29*). For our experimental parameters (C = 0.46, N = 61, where N is the average number of loaded spectator qubits) we find $f \approx 0.88$, in good agreement with the numerical simulations.

In the context of quantum information processing, it is interesting to consider the requirements to reach $f \gg 0.99$. Without any change in γ or β, $f = 0.99$ could be achieved for N = 165 and C = 1. At present, the value of C is limited primarily by uncorrelated dephasing of the spectator qubits, caused by thermal motion in the optical tweezers and tweezer-induced T_1 processes. Thermal motion can be reduced by additional cooling schemes and T_1 can be improved by increased detuning of the optical tweezers.

Beyond optimizing for $\gamma \approx 1$, f can be further improved by reducing β, at the cost of a reduced range of correctable data qubit errors, $\Phi_{D,max} = \pm\gamma\beta\pi/2$. This could be achieved with alternative spectator qubit states, such as magnetic-field-sensitive states.

Although here we focus on magnetic field noise, the protocol can also mitigate common-mode control errors. For instance, by co-trapping the data and spectator qubits using the same laser system (such as a far-detuned 1064 nm laser), phase errors induced by intensity fluctuations of the trapping laser light could be corrected.

Coherent reloading of spectator qubits

In these experiments, fluorescence-based detection of the spectators involves selectively removing those in the $|1\rangle_{Cs}$ state prior to imaging. Therefore, performing repetitive MCRs will continuously deplete the array. Although low-loss readout techniques exist (*30*, *31*), finite losses always remain from both the readout itself and the trapping lifetime. Therefore, continuous operation of atom-based quantum processors will require reload and reset operations which overcome these erasure errors (*32*, *33*). Here, we explore two methods for reloading spectators while maintaining coherent data qubits. These build on our standard procedure, where a two-dimensional magneto-optical trap generates a beam of atoms that is laser-cooled into the tweezer array via a three-dimensional magneto-optical trap (MOT).

The first reloading approach uses a stroboscopic MOT that is applied synchronously with an XY4 sequence on the data qubits, to decouple them from the magnetic field gradient (Fig. 4A). Without the gradient, this decoupling sequence gives T_2^{XY4} = 0.45(1) s. With it, we find T_2^{XY4} = 0.42(3) s, but the functional form is modified (*29*). The spectator array is reloaded on a much shorter timescale of 150(50) ms, defined as the time taken to reach 1 − 1/e of the asymptotic loading fraction. The pulsed MOT saturates at a loading fraction of

0.49, comparable to that achieved with the standard procedure. Residual dephasing from the field gradient can be overcome by using low inductance coils with faster switching times, and by performing decoupling pulses using a Raman laser system, which would enable ~MHz Rabi frequencies.

In the second approach, we use polarization-gradient cooling (PGC) to load spectators directly from the atomic beam without a field gradient (Fig. 4B). This both increases the loading speed and allows an arbitrary choice of decoupling parameters: here we use a single cycle of XY8. In this reloading paradigm, the data qubit coherence time [T_2^{XY8} = 0.64(5) s] is unchanged from the values presented in Fig. 2, and the spectator qubit array is reloaded on a timescale of 90(30) ms. The fraction of total reloaded spectators is lower than in the previous method, saturating at 0.32. We hypothesize that this is limited by the 2 mm diameter cooling beams. Incorporating larger cooling beams will likely increase the loading fraction for both approaches and would enable reloading times of a few tens of milliseconds (*34*). Coherence times of ~ seconds can be achieved by using further detuned trapping light and a larger number of decoupling pulses (*9*).

Discussion and outlook

A central challenge for all quantum architectures is to increase system sizes while maintaining low physical error rates. Our demonstration of the use of spectator qubits to measure and correct correlated phase noise is a broadly applicable strategy that can be employed to reduce error rates in quantum computing platforms. Furthermore, spectator protocols could be used in conjunction with standard quantum error correction strategies to protect against correlated errors as well as increase the fidelity of operations beyond the fault-tolerance threshold. An attractive feature of this protocol is that it does not necessitate interactions (two-qubit gates), or individual spectator qubit control, reducing hardware complexity. The use of spectator qubits for noise measurements may provide opportunities in quantum sensing and metrology (*22*, *35*, *36*), and for improving clock coherence within a single device via differential spectroscopy between the data and spectator qubits (*37*). Whereas here we focus on global noise, arrays of spectator qubits may also enable the detection of spatially varying noise fields which can be suppressed via local qubit addressing (*24*). Careful engineering of the spectator qubits and their control sequences may improve protocol performance. For example, spectator qubits could be encoded in states with enhanced or reduced noise sensitivity to increase the phase resolution or the range of tolerable noise (*25*). This can be achieved by using nonzero m_F states or by entangling the spectator qubits (*22*).

The methods demonstrated in this work constitute a set of quantum-control techniques that are essential for atom-array quantum processors, including mid-circuit readout, feed-forward operations, and reloading of auxiliary qubits while maintaining quantum data. Combining these capabilities with programmable intraspecies (*9*, *38*) and interspecies Rydberg gates will enable auxiliary-qubit-assisted measurements as required for quantum error correction (*32*, *33*, *39*) and efficient preparation of long-range entangled states (*40*). These same capabilities also enable the exploration of complex dynamical quantum behavior under continuous observation, including measurement-induced phase transitions (*41*).

Note added in proof: After the consideration of this manuscript, a pre-print was published describing mid-circuit read-out of a neutral atom by shelving in hyperfine states (*42*).

REFERENCES AND NOTES

1. E. T. Campbell, B. M. Terhal, C. Vuillot, Roads towards fault-tolerant universal quantum computation. *Nature* **549**, 172–179 (2017). doi:10.1038/nature23460 Medline
2. B. M. Terhal, Quantum error correction for quantum memories. *Rev. Mod. Phys.* **87**, 307–346 (2015). doi:10.1103/RevModPhys.87.307
3. C. Ryan-Anderson, J. G. Bohnet, K. Lee, D. Gresh, A. Hankin, J. P. Gaebler, D. Francois, A. Chernoguzov, D. Lucchetti, N. C. Brown, T. M. Gatterman, S. K. Halit, K. Gilmore, J. A. Gerber, B. Neyenhuis, D. Hayes, R. P. Stutz, Realization of real-time fault-tolerant quantum error correction. *Phys. Rev. X* **11**, 041058 (2021). doi:10.1103/PhysRevX.11.041058
4. L. Postler, S. Heuβen, I. Pogorelov, M. Rispler, T. Feldker, M. Meth, C. D. Marciniak, R. Stricker, M. Ringbauer, R. Blatt, P. Schindler, M. Müller, T. Monz, Demonstration of fault-tolerant universal quantum gate operations. *Nature* **605**, 675–680 (2022). doi:10.1038/s41586-022-04721-1 Medline
5. Y. Zhao, Y. Ye, H.-L. Huang, Y. Zhang, D. Wu, H. Guan, Q. Zhu, Z. Wei, T. He, S. Cao, F. Chen, T.-H. Chung, H. Deng, D. Fan, M. Gong, C. Guo, S. Guo, L. Han, N. Li, S. Li, Y. Li, F. Liang, J. Lin, H. Qian, H. Rong, H. Su, L. Sun, S. Wang, Y. Wu, Y. Xu, C. Ying, J. Yu, C. Zha, K. Zhang, Y.-H. Huo, C.-Y. Lu, C.-Z. Peng, X. Zhu, J.-W. Pan, Realization of an error-correcting surface code with superconducting qubits. *Phys. Rev. Lett.* **129**, 030501 (2022). doi:10.1103/PhysRevLett.129.030501 Medline
6. S. Krinner, N. Lacroix, A. Remm, A. Di Paolo, E. Genois, C. Leroux, C. Hellings, S. Lazar, F. Swiadek, J. Herrmann, G. J. Norris, C. K. Andersen, M. Müller, A. Blais, C. Eichler, A. Wallraff, Realizing repeated quantum error correction in a distance-three surface code. *Nature* **605**, 669–674 (2022). doi:10.1038/s41586-022-04566-8 Medline
7. R. Acharya, I. Aleiner, R. Allen, T. I. Andersen, M. Ansmann, F. Arute, K. Arya, A. Asfaw, J. Atalaya, R. Babbush, D. Bacon, J. C. Bardin, J. Basso, A. Bengtsson, S. Boixo, G. Bortoli, A. Bourassa, J. Bovaird, L. Brill, M. Broughton, B. B. Buckley, D. A. Buell, T. Burger, B. Burkett, N. Bushnell, Y. Chen, Z. Chen, B. Chiaro, J. Cogan, R. Collins, P. Conner, W. Courtney, A. L. Crook, B. Curtin, D. M. Debroy, A. Del Toro Barba, S. Demura, A. Dunsworth, D. Eppens, C. Erickson, L. Faoro, E. Farhi, R. Fatemi, L. Flores Burgos, E. Forati, A. G. Fowler, B. Foxen, W. Giang, C. Gidney, D. Gilboa, M. Giustina, A. Grajales Dau, J. A. Gross, S. Habegger, M. C. Hamilton, M. P. Harrigan, S. D. Harrington, O. Higgott, J. Hilton, M. Hoffmann, S. Hong, T. Huang, A. Huff, W. J. Huggins, L. B. Ioffe, S. V. Isakov, J. Iveland, E. Jeffrey, Z. Jiang, C. Jones, P. Juhas, D. Kafri, K. Kechedzhi, J. Kelly, T. Khattar, M. Khezri, M. Kieferová, S. Kim, A. Kitaev, P. V. Klimov, A. R. Klots, A. N. Korotkov, F. Kostritsa, J. M. Kreikebaum, D. Landhuis, P. Laptev, K.-M. Lau, L. Laws, J. Lee, K. Lee, B. J. Lester, A. Lill, W. Liu, A. Locharla, E. Lucero, F. D. Malone, J. Marshall, O. Martin, J. R. McClean, T. McCourt, M. McEwen, A. Megrant, B. Meurer Costa, X. Mi, K. C. Miao, M. Mohseni, S. Montazeri, A. Morvan, E. Mount, W. Mruczkiewicz, O. Naaman, M. Neeley, C. Neill, A. Nersisyan, H. Neven, M. Newman, J. H. Ng, A. Nguyen, M. Nguyen, M. Y. Niu, T. E. O'Brien, A. Opremcak, J. Platt, A. Petukhov, R. Potter, L. P. Pryadko, C. Quintana, P. Roushan, N. C. Rubin, N. Saei, D. Sank, K. Sankaragomathi, K. J. Satzinger, H. F. Schurkus, C. Schuster, M. J. Shearn, A.

Shorter, V. Shvarts, J. Skruzny, V. Smelyanskiy, W. C. Smith, G. Sterling, D. Strain, M. Szalay, A. Torres, G. Vidal, B. Villalonga, C. Vollgraff Heidweiller, T. White, C. Xing, Z. J. Yao, P. Yeh, J. Yoo, G. Young, A. Zalcman, Y. Zhang, N. Zhu; Google Quantum AI, Suppressing quantum errors by scaling a surface code logical qubit. *Nature* **614**, 676–681 (2023). doi:10.1038/s41586-022-05434-1 Medline

8. M. H. Abobeih, Y. Wang, J. Randall, S. J. H. Loenen, C. E. Bradley, M. Markham, D. J. Twitchen, B. M. Terhal, T. H. Taminiau, Fault-tolerant operation of a logical qubit in a diamond quantum processor. *Nature* **606**, 884–889 (2022). doi:10.1038/s41586-022-04819-6 Medline
9. D. Bluvstein, H. Levine, G. Semeghini, T. T. Wang, S. Ebadi, M. Kalinowski, A. Keesling, N. Maskara, H. Pichler, M. Greiner, V. Vuletić, M. D. Lukin, A quantum processor based on coherent transport of entangled atom arrays. *Nature* **604**, 451–456 (2022). doi:10.1038/s41586-022-04592-6 Medline
10. J. Preskill, Sufficient condition on noise correlations for scalable quantum computing. *Quantum Inf. Comput.* **13**, 181–194 (2013). doi:10.26421/QIC13.3-4-1
11. A. G. Fowler, J. M. Martinis, Quantifying the effects of local many-qubit errors and nonlocal two-qubit errors on the surface code. *Phys. Rev. A* **89**, 032316 (2014). doi:10.1103/PhysRevA.89.032316
12. S. Kuhr, W. Alt, D. Schrader, I. Dotsenko, Y. Miroshnychenko, A. Rauschenbeutel, D. Meschede, Analysis of dephasing mechanisms in a standing-wave dipole trap. *Phys. Rev. A* **72**, 023406 (2005). doi:10.1103/PhysRevA.72.023406
13. T. Monz, P. Schindler, J. T. Barreiro, M. Chwalla, D. Nigg, W. A. Coish, M. Harlander, W. Hänsel, M. Hennrich, R. Blatt, 14-Qubit entanglement: Creation and coherence. *Phys. Rev. Lett.* **106**, 130506 (2011). doi:10.1103/PhysRevLett.106.130506 Medline
14. C. E. Bradley, J. Randall, M. H. Abobeih, R. C. Berrevoets, M. J. Degen, M. A. Bakker, M. Markham, D. J. Twitchen, T. H. Taminiau, A ten-qubit solid-state spin register with quantum memory up to one minute. *Phys. Rev. X* **9**, 031045 (2019). doi:10.1103/PhysRevX.9.031045
15. J. M. Boter, X. Xue, T. Krähenmann, T. F. Watson, V. N. Premakumar, D. R. Ward, D. E. Savage, M. G. Lagally, M. Friesen, S. N. Coppersmith, M. A. Eriksson, R. Joynt, L. M. K. Vandersypen, Spatial noise correlations in a Si/SiGe two-qubit device from Bell state coherences. *Phys. Rev. B* **101**, 235133 (2020). doi:10.1103/PhysRevB.101.235133
16. C. D. Wilen, S. Abdullah, N. A. Kurinsky, C. Stanford, L. Cardani, G. D'Imperio, C. Tomei, L. Faoro, L. B. Ioffe, C. H. Liu, A. Opremcak, B. G. Christensen, J. L. DuBois, R. McDermott, Correlated charge noise and relaxation errors in superconducting qubits. *Nature* **594**, 369–373 (2021). doi:10.1038/s41586-021-03557-5 Medline
17. L. M. Vandersypen, I. L. Chuang, NMR techniques for quantum control and computation. *Rev. Mod. Phys.* **76**, 1037–1069 (2005). doi:10.1103/RevModPhys.76.1037
18. H. A. Rabitz, M. M. Hsieh, C. M. Rosenthal, Quantum optimally controlled transition landscapes. *Science* **303**, 1998–2001 (2004). doi:10.1126/science.1093649 Medline
19. T. Gullion, D. B. Baker, M. S. Conradi, New, compensated Carr-Purcell sequences. *J. Magn. Reson.* **89**, 479–484 (1990). doi:10.1016/0022-2364(90)90331-3
20. M. D. Shulman, S. P. Harvey, J. M. Nichol, S. D. Bartlett, A. C. Doherty, V. Umansky, A. Yacoby, Suppressing qubit dephasing using real-time Hamiltonian estimation. *Nat. Commun.* **5**, 5156 (2014). doi:10.1038/ncomms6156 Medline
21. S. Mavadia, V. Frey, J. Sastrawan, S. Dona, M. J. Biercuk, Prediction and real-time compensation of qubit decoherence via machine learning. *Nat. Commun.* **8**, 14106 (2017). doi:10.1038/ncomms14106 Medline
22. C. L. Degen, F. Reinhard, P. Cappellaro, Quantum sensing. *Rev. Mod. Phys.* **89**, 035002 (2017). doi:10.1103/RevModPhys.89.035002
23. S. Majumder, L. Andreta de Castro, K. R. Brown, Real-time calibration with spectator qubits. *NPJ Quantum Inf.* **6**, 19 (2020). doi:10.1038/s41534-020-0251-y
24. R. S. Gupta, L. C. Govia, M. J. Biercuk, Integration of spectator qubits into quantum computer architectures for hardware tune-up and calibration. *Phys. Rev. A* **102**, 042611 (2020). doi:10.1103/PhysRevA.102.042611
25. H. Song, A. Chantasri, B. Tonekaboni, H. M. Wiseman, Optimized mitigation of random-telegraph-noise dephasing by spectator-qubit sensing and control. *Phys. Rev. A* **107**, L030601 (2023). doi:10.1103/PhysRevA.107.L030601
26. K. Singh, S. Anand, A. Pocklington, J. T. Kemp, H. Bernien, Dual-element, two-dimensional atom array with continuous-mode operation. *Phys. Rev. X* **12**, 011040 (2022). doi:10.1103/PhysRevX.12.011040
27. E. Deist, Y.-H. Lu, J. Ho, M. K. Pasha, J. Zeiher, Z. Yan, D. M. Stamper-Kurn, Mid-circuit cavity measurement in a neutral atom array. *Phys. Rev. Lett.* **129**, 203602 (2022). doi:10.1103/PhysRevLett.129.203602 Medline
28. J. T. Zhang, L. R. B. Picard, W. B. Cairncross, K. Wang, Y. Yu, F. Fang, K.-K. Ni, An optical tweezer array of ground-state polar molecules. *Quantum Sci. Technol.* **7**, 035006 (2022). doi:10.1088/2058-9565/ac676c
29. See supplementary materials.
30. A. Fuhrmanek, R. Bourgain, Y. R. P. Sortais, A. Browaeys, Free-space lossless state detection of a single trapped atom. *Phys. Rev. Lett.* **106**, 133003 (2011). doi:10.1103/PhysRevLett.106.133003 Medline
31. M. J. Gibbons, C. D. Hamley, C.-Y. Shih, M. S. Chapman, Nondestructive fluorescent state detection of single neutral atom qubits. *Phys. Rev. Lett.* **106**, 133002 (2011). doi:10.1103/PhysRevLett.106.133002 Medline
32. I. Cong, H. Levine, A. Keesling, D. Bluvstein, S.-T. Wang, M. D. Lukin, Hardware-efficient, fault-tolerant quantum computation with Rydberg atoms. *Phys. Rev. X* **12**, 021049 (2022). doi:10.1103/PhysRevX.12.021049
33. Y. Wu, S. Kolkowitz, S. Puri, J. D. Thompson, Erasure conversion for fault-tolerant quantum computing in alkaline earth Rydberg atom arrays. *Nat. Commun.* **13**, 4657 (2022). doi:10.1038/s41467-022-32094-6 Medline
34. A. Steane, M. Chowdhury, C. Foot, Radiation force in the magneto-optical trap. *J. Opt. Soc. Am. B* **9**, 2142 (1992). doi:10.1364/JOSAB.9.002142
35. I. S. Madjarov, A. Cooper, A. L. Shaw, J. P. Covey, V. Schkolnik, T. H. Yoon, J. R. Williams, M. Endres, An atomic-array optical clock with single-atom readout. *Phys. Rev. X* **9**, 041052 (2019). doi:10.1103/PhysRevX.9.041052
36. M. A. Norcia, A. W. Young, W. J. Eckner, E. Oelker, J. Ye, A. M. Kaufman, Seconds-scale coherence on an optical clock transition in a tweezer array. *Science* **366**, 93–97 (2019). doi:10.1126/science.aay0644 Medline
37. M. E. Kim, W. F. McGrew, N. V. Nardelli, E. R. Clements, Y. S. Hassan, X. Zhang, J. L. Valencia, H. Leopardi, D. B. Hume, T. M. Fortier, A. D. Ludlow, D. R. Leibrandt, Improved interspecies optical clock comparisons through differential spectroscopy. *Nat. Phys.* **19**, 25–29 (2023). doi:10.1038/s41567-022-01794-7
38. T. M. Graham, Y. Song, J. Scott, C. Poole, L. Phuttitarn, K. Jooya, P. Eichler, X. Jiang, A. Marra, B. Grinkemeyer, M. Kwon, M. Ebert, J. Cherek, M. T. Lichtman, M. Gillette, J. Gilbert, D. Bowman, T. Ballance, C. Campbell, E. D. Dahl, O. Crawford, N. S. Blunt, B. Rogers, T. Noel, M. Saffman, Multi-qubit entanglement and algorithms on a neutral-atom quantum computer. *Nature* **604**, 457–462 (2022). doi:10.1038/s41586-022-04603-6 Medline
39. M. Morgado, S. Whitlock, Quantum simulation and computing with Rydberg-interacting qubits. *AVS Quantum Sci.* **3**, 023501 (2021). doi:10.1116/5.0036562
40. R. Verresen, N. Tantivasadakarn, A. Vishwanath, Efficiently preparing Schrödinger's cat, fractons and non-Abelian topological order in quantum devices. arXiv:2112.03061 [quant-ph] (2021).
41. Y. Li, X. Chen, M. P. A. Fisher, Quantum Zeno effect and the many-body entanglement transition. *Phys. Rev. B* **98**, 205136 (2018). doi:10.1103/PhysRevB.98.205136
42. T. M. Graham, L. Phuttitarn, R. Chinnarasu, Y. Song, C. Poole, K. Jooya, J. Scott, A. Scott, P. Eichler, M. Saffman, Mid-circuit measurements on a neutral atom quantum processor. arXiv:2303.10051 [quant-ph] (2023).
43. K. Singh, C. Bradley, S. Anand, V. Ramesh, R. White, H. Bernien, Data and plotting code for "Mid-circuit correction of correlated phase errors using an array of spectator qubits". Zenodo (2023); https://doi.org/10.5281/zenodo.7612718.
44. H. Levine, A. Keesling, G. Semeghini, A. Omran, T. T. Wang, S. Ebadi, H. Bernien, M. Greiner, V. Vuletić, H. Pichler, M. D. Lukin, Parallel implementation of high-fidelity multiqubit gates with neutral atoms. *Phys. Rev. Lett.* **123**, 170503 (2019). doi:10.1103/PhysRevLett.123.170503 Medline
45. M. E. Shea, P. M. Baker, J. A. Joseph, J. Kim, D. J. Gauthier, Submillisecond, nondestructive, time-resolved quantum-state readout of a single, trapped neutral atom. *Phys. Rev. A* **102**, 053101 (2020). doi:10.1103/PhysRevA.102.053101
46. P. Yang, G. Li, Z. Wang, P. Zhang, T. Zhang, Gate fidelity, dephasing, and 'magic' trapping of optically trapped neutral atom. *New J. Phys.* **24**, 083028 (2022). doi:10.1088/1367-2630/ac87ca
47. D. A. Steck, Rubidium 87 D line data (2001); https://steck.us/alkalidata/rubidium87numbers.1.6.pdf.
48. D. A. Steck, Cesium D line data (2003);

https://steck.us/alkalidata/cesiumnumbers.1.6.pdf.

ACKNOWLEDGMENTS

We thank Harry Levine, Jacob Covey, and Aashish Clerk for fruitful discussions and critical reading of the manuscript. **Funding:** We acknowledge funding from the Office for Naval Research (N00014-20-1-2510), the Air Force Office of Scientific Research (FA9550-21-1-0209), the NSF QLCI for Hybrid Quantum Architectures and Networks (NSF award 2016136), and the Sloan Foundation. This material is based upon work supported by the U.S. Department of Energy Office of Science National Quantum Information Science Research Centers and was supported by an appointment to the Intelligence Community Postdoctoral Research Fellowship Program at the Pritzker School of Molecular Engineering administered by Oak Ridge Institute for Science and Education through an interagency agreement between the U.S. Department of Energy and the Office of the Director of National Intelligence. **Author contributions:** K.S., C.E.B., S.A., V.R., R.W., and H.B. contributed to the experiments. K.S., C.E.B, S.A., and H.B. contributed to analysis of the results and preparation of the manuscript. **Competing interests:** The work described in this article is included in a patent application filed with the US Patent and Trade Office by the University of Chicago. **Data and materials availability:** The data and code supporting this study is available at (*43*).

SUPPLEMENTARY MATERIALS
science.org/doi/10.1126/science.ade5337
Materials and Methods
Supplementary Text
Figs. S1 to S5
Tables S1 and S2
References (*44*–*48*)

Submitted 24 August 2022; accepted 15 May 2023
Published online 25 May 2023
10.1126/science.ade5337

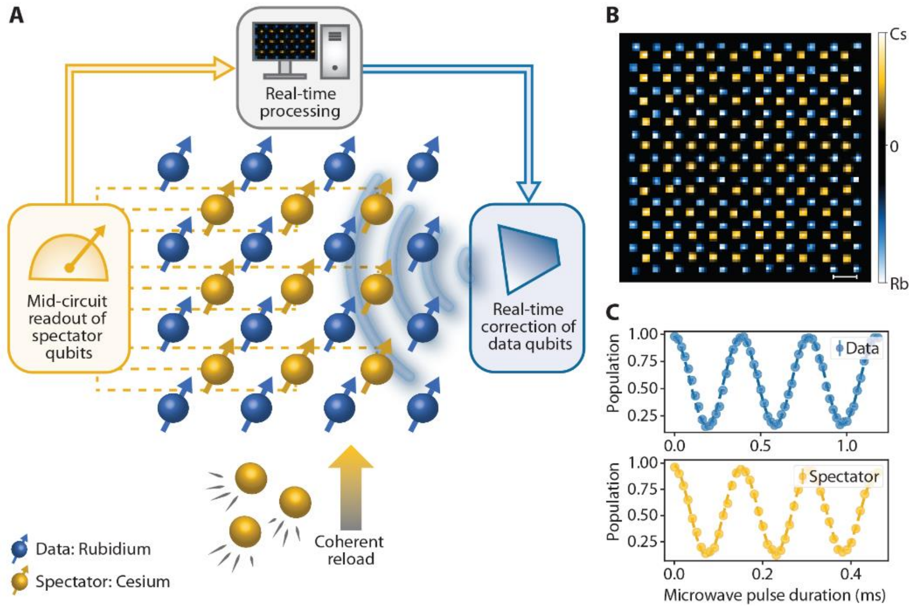

Fig. 1. Spectator qubit protocol with a dual-species atom array. (**A**) Feed-forward loop for real-time correction of correlated phase errors between data qubits (Rb atoms, blue) and spectator qubits (Cs atoms, yellow). A mid-circuit, single-shot phase estimation on the spectators is used to infer the noise-induced phase accrued by the data qubits. This information enables a real-time correction on the data qubits prior to the final readout, suppressing dephasing. Subsequently, spectator qubits lost during readout can be replenished while maintaining data qubit coherence. (**B**) Example fluorescence image of the dual-species atom array. Scale-bar indicates ~10 μm. (**C**) Microwave Rabi oscillations of the data and spectator qubits. Dashed lines are fits to exponentially decaying sinusoids.

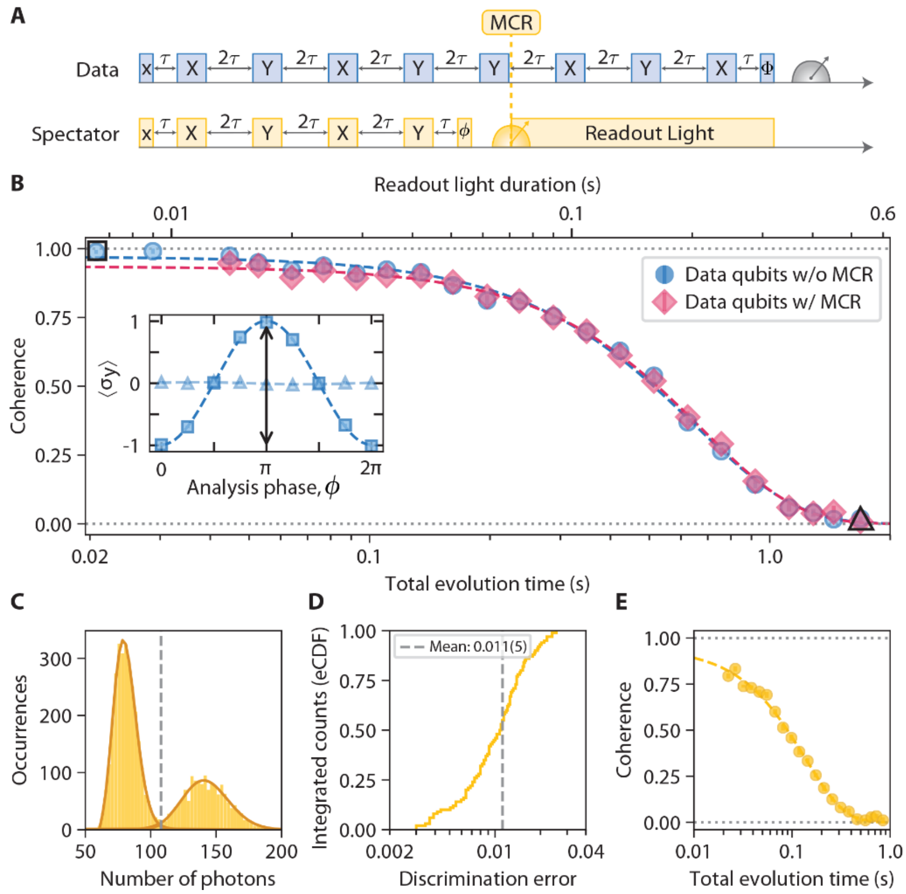

Fig. 2. Mid-circuit readout of atomic qubits. (**A**) Pulse diagram depicting mid-circuit readout (MCR) of atomic qubits. Lower case and upper case letters indicate π/2 and π pulses, respectively, along that axis of rotation. Readout light is left on for the remaining duration of the sequence after MCR. (**B**) Measurement of spectator qubit dynamics while preserving data qubit coherence. During an XY8 decoupling sequence on the data qubits (red diamonds), we perform an XY4 decoupling sequence and subsequent projective measurement on the spectator qubits. The data qubit coherence ($\sqrt{\langle\sigma_x\rangle^2+\langle\sigma_y\rangle^2}$) is unchanged in the absence of MCR (blue circles). Dashed lines are fits (*29*). Inset: coherence measurements for early (square) and late (triangle) evolution times. (**C**) Example fluorescence histogram of a spectator qubit. Solid lines are fits to a bimodal Poisson distribution. (**D**) Cumulative histogram of the discrimination infidelities of the spectator qubits during mid-circuit readout (*29*). (**E**) Coherence of spectator qubits. The measured spectator coherence time is $T_2^{XY4}=136(7)$ ms.

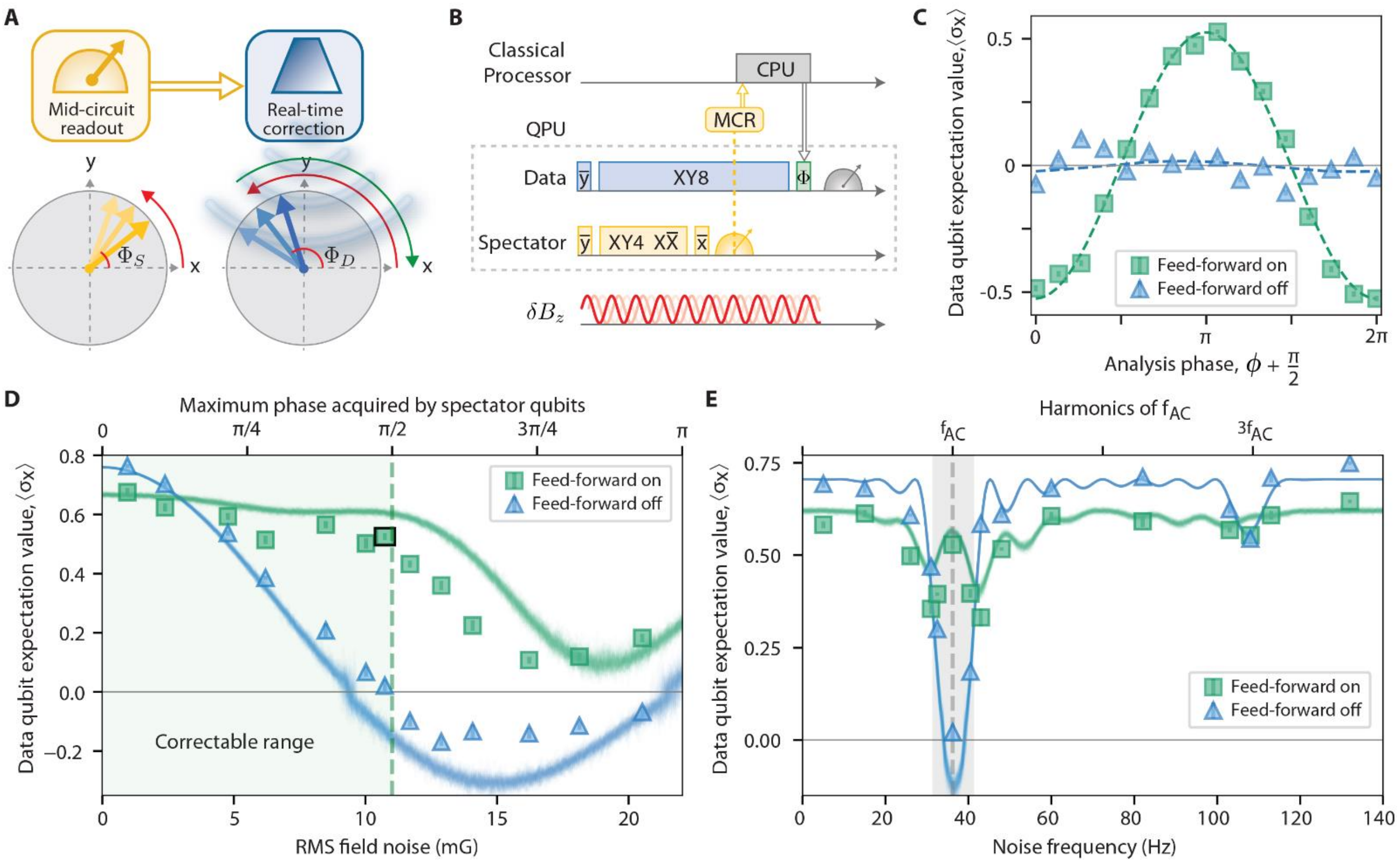

Fig. 3. Mid-circuit correction of correlated phase errors. (**A**) Noise channels induce correlated phase errors (red arrows) between the two sets of qubits. Measurement of the spectators along the y-axis enables single-shot phase estimation, from which the phase accrued by the data qubits can be inferred and corrected in real-time. (**B**) Gate sequence. The data and spectator qubits are synchronously decoupled and acquire correlated errors owing to magnetic field noise δB_z. The spectator qubit decoupling sequence is truncated, with the remaining time assigned for mid-circuit readout and feed-forward. (**C**) Example coherence measurement of the data qubits at the end of the sequence, with the feed-forward turned on (green squares) and off (blue triangles). Field noise is applied at f_{AC} = 36.2 Hz, 10.7 mG RMS. Dashed lines are fits, from which we extract $\langle \sigma_x \rangle$ = 0.53(1) and 0.02(2), respectively. (**D**) Data qubit $\langle \sigma_x \rangle$ as a function of the RMS noise strength at f_{AC}. The shaded green region indicates the correctable range (see text). (**E**) Data qubit $\langle \sigma_x \rangle$ as a function of the noise frequency at 10.7 mG RMS. Shaded grey region indicates an absolute gain in the measured coherence. For (D) and (E), solid lines are the results of numerical simulations (see text).

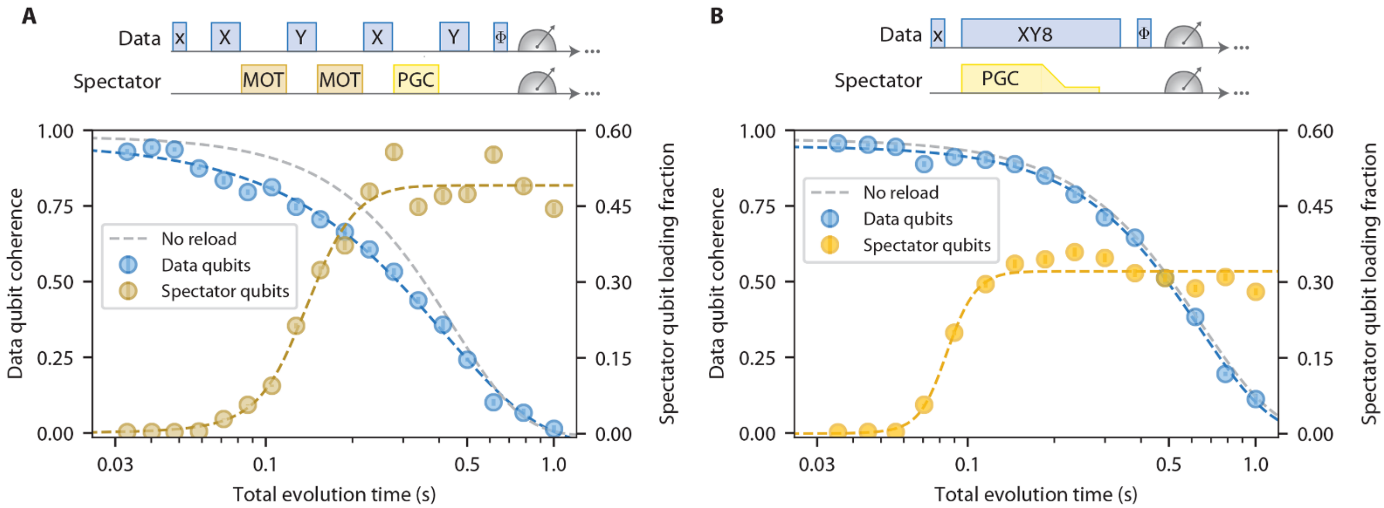

Fig. 4. Reloading of spectator qubits while maintaining data qubit coherence. (**A**) Reloading spectators using a pulsed magneto-optical trap (MOT) while decoupling the data qubits. The data qubit coherence time is T_2^{XY4} = 0.42(3) s with the pulsed MOT and T_2^{XY4} = 0.45(1) s without it. Spectators are reloaded on a timescale of 150(50) ms (time required to reach 1 – 1/*e* of asymptote), saturating at a loading fraction of 0.49. (**B**) Reloading spectators using polarization-gradient cooling (PGC) during data qubit decoupling. The data qubit coherence time is T_2^{XY8} = 0.64(5) s with the PGC light, and T_2^{XY8} = 0.65(2) s without it. Reloading occurs on a faster timescale of 90(30) ms compared to (A), saturating at a fraction of 0.32. Dashed lines are fits (*29*).

Mid-circuit correction of correlated phase errors using an array of spectator qubits

K. Singh, C. E. Bradley, S. Anand, V. Ramesh, R. White, and H. Bernien

Science,**Ahead of Print**
DOI: 10.1126/science.ade5337